CHEMISTRY
A European Journal

A Journal of
ChemPubSoc Europe

## Accepted Article

**Title:** Metal···F–C bonding in low-coordinate alkaline-earth fluoroarylamides

**Authors:** Yann Sarazin, Hanieh Roueindeji, Antsa Ratsifitahina, Thierry Roisnel, Vincent Dorcet, Samia Kahlal, Jean-Yves Saillard, and Jean-François Carpentier



**To be cited as:** *Chem. Eur. J.* 10.1002/chem.201901262

**Link to VoR:** http://dx.doi.org/10.1002/chem.201901262

Supported by
ACES

WILEY-VCH

10.1002/chem.201901262

# Metal···F–C bonding in low-coordinate alkaline-earth fluoroarylamides

Hanieh Roueindeji, Antsa Ratsifitahina, Thierry Roisnel, Vincent Dorcet, Samia Kahlal, Jean-Yves Saillard,* Jean-François Carpentier and Yann Sarazin*[a]

[a] Univ Rennes, CNRS, ISCR (Institut des Sciences Chimiques de Rennes) – UMR 6226, F-35000 Rennes, France.

Corresponding authors: yann.sarazin@univ-rennes1.fr; jean-yves.saillard@univ-rennes1.fr



**Keywords:** calcium • alkaline earth metals • low coordinate complexes • DFT computations • metal-fluorine bonding

10.1002/chem.201901262


## Abstract

A set of calcium and barium complexes containing the fluoroarylamide $N(C_6F_5)_2^-$ is presented. These compounds illustrate the key role of stabilising M···F–C secondary interactions in the construction of low coordinate alkaline earth complexes. The nature of Ca···F–C bonding in calcium complexes is examined in the light of structural data, bond valence sum analysis (BVSA) and DFT computations. The molecular structures of $[Ca\{N(C_6F_5)_2\}_2.(Et_2O)_2]$ (**4'**), $[Ca\{\mu^2\text{-}N(SiMe_3)_2\}\{N(C_6F_5)_2\}]_2$ (**5₂**), $[Ba\{\mu\text{-}N(C_6F_5)_2\}\{N(C_6F_5)_2\}.toluene]_2$ (**6₂**), $[\{BDI^{DiPP}\}CaN(C_6F_5)_2]_2$ (**7₂**), $[\{N\text{^}N^{DiPP}\}CaN(C_6F_5)_2]_2$ (**8₂**), and $[Ca\{\mu\text{-}OB(CH(SiMe_3)_2)_2\}\{N(C_6F_5)_2\}]_2$ (**9₂**), where $\{BDI^{DiPP}\}^-$ and $\{N\text{^}N^{DiPP}\}^-$ are the bidentate ligands $CH[C(CH_3)NDipp]_2$ and $DippNC_6H_4CNDipp$ (Dipp = 2,6-*i*$Pr_2$-$C_6H_3$), are detailed. Complex **6₂** displays strong Ba···F–C contacts at ca. 2.85 Å. The calcium complexes feature also very short intramolecular Ca-F interatomic distances, at around 2.50 Å. Besides, the three-coordinate complexes **7₂** and **9₂** form dinuclear edifices due to *intermolecular* Ca···F–C contacts. BVSA shows that Ca···F–C interactions contribute to 15-20% of the bonding pattern around calcium. Computations demonstrate that Ca···F–C bonding is mostly electrostatic, but also contains a non-negligible covalent contribution. They also suggest that Ca···F–C are the strongest amongst the range of weak Ca···X (X = F, H, C$\pi$) secondary interactions, owing to the high positive charge of $Ca^{2+}$ which favours electrostatic interactions.

10.1002/chem.201901262

## Introduction

Well defined, soluble complexes of the abundant large alkaline earths calcium, strontium and barium (= Ae metals) have of late emerged as viable alternative to mainstream homogenous catalysts based on expensive late transition metals.[1] A panel of molecular Ca-Ba precatalysts featuring a controlled coordination sphere tailored around bulky, multidentate and often monoanionic ligands are now available for the catalysis of a growing range of transformations such as hydroelementations,[2] dehydrocouplings[3] or polymerisations.[4] Complexes of these metals also promote remarkable cases of stoichiometric or subcatalytic functionalisations of small molecules.[5] The pronounced electrophilicity of the metal in low coordinate Ae complexes is often the main driving force behind the efficiency of these systems. Ae metals are large ($r_{ionic}$ = 1.00, 1.18 and 1.35 Å for Ca, Sr and Ba in a coordination number of 6), electropositive elements (with their respective Pauling electronegativity of 1.00, 0.95 and 0.89) that generate complexes where the bonding pattern around the dication $Ae^{2+}$ is governed by electrostatic and steric factors, with little propensity for orbital contributions. The perennial search for low coordinate complexes offering the best compromise between stability and reactivity has triggered the design of multidentate ligands based on *O*- or *N*-donors that match the hard, oxophilic nature of Ae metals. The ubiquitous, bidentate β-diketiminate $\{BDI^{DiPP}\}^-$ (where $BDI^{DiPP}$ = $CH[C(CH_3)NDipp]_2$, Dipp = 2,6-diisopropylphenyl, Figure 1) has proved exceptionally successful in enabling access to highly reactive, low coordinate Ae species,[1-6] with the four-coordinate $[\{BDI^{DiPP}\}CaN(SiMe_3)_2.(thf)]$ (**1**) proving a notably versatile and potent precatalyst.[1] Related complexes were subsequently devised, and the sterically hindered iminoanilido ligand $\{N\text{^}N^{DiPP}\}^-$ for instance afforded $[\{N\text{^}N^{DiPP}\}CaN(SiMe_3)_2.(thf)]$ (**2**), an excellent precatalyst for the cyclohydroamination of α,ω-aminoalkenes.[7] Yet, because it reduces electrophilicity of the metal ion and might inhibit coordination of an incoming substrate, the presence of coordinated thf in **1** and **2** and related complexes often proves detrimental to catalytic turnovers or stoichiometric reactivity studies.[1] This is perhaps best epitomised by Hill's recent demonstration that $[\{BDI^{DiPP}\}CaH]_2$ (made from solvent-free $[\{BDI^{DiPP}\}CaN(SiMe_3)_2]$ (**3**)[8]) inserts non-activated α-olefins to generate $[\{BDI^{DiPP}\}CaR]_2$ Ca-alkyl species, while $[\{BDI^{DiPP}\}CaH.(thf)]_2$ is comparatively inert.[2j,6e]

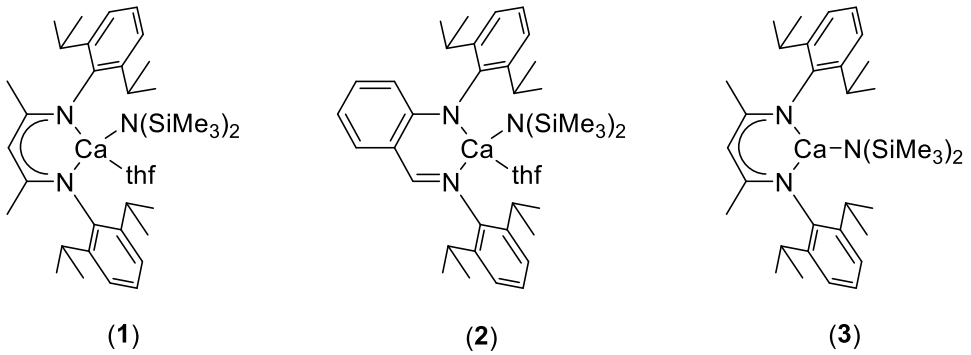


(**1**) (**2**) (**3**)

**Figure 1** Examples of low-coordinate calcium complexes bearing chelating N-based ligands.

10.1002/chem.201901262

It has been shown on repeated occasions that the removal of coordinated solvent molecules was a valuable strategy in order to obtain low-coordinate Ae compounds. The implementation of secondary interactions has been a driving force in this purpose,[9] and a variety of unusual complexes stabilised by β-agostic Ae···H–Si,[10] Ae···C(π)[11] or, perhaps most importantly, Ae···F–C[12] non-covalent interactions, is now available. Many of them have been used to great effect as molecular precatalysts.[1] In this context, fluorinated amines have been used to obtain low coordinate, homoleptic synthetic precursors of electrophilic elements (Figure 2). $Sm[N(C_6F_5)(SiMe_3)]_3$ exhibited three intramolecular Sm···F–C contacts.[13] The Schelter group prepared U(III), U(IV) and Ce(III) complexes bearing various fluorinated arylamides, notably $N(C_6F_5)_2^-$ and $N(SiMe_3)(o\text{-}F\text{-}C_6H_4)^-$, that feature several stabilising metal···F–C contacts.[14] Sundermeyer and coworkers pioneered this theme in main group metal chemistry. They prepared volatile magnesium and alkali salts of the mixed $N(C_6F_5)(C(CF_3)_3)^-$ amide,[15] and also reported on the highly Lewis acidic $Al[N(C_6F_5)_2]_3$ and $Ga[N(C_6F_5)_2]_3$.[16] Prior to this, Westerhausen had utilised 2,6-difluoroanilide to synthesise multinuclear complexes that exhibit intra- and intermolecular Ae···F–C contacts (Ae = Sr or Ba), such as the one-dimensional polymer $[(thf)_2Ba\{N(H)\text{-}2,6\text{-}F_2\text{-}C_6H_3\}]_\infty$.[12b]

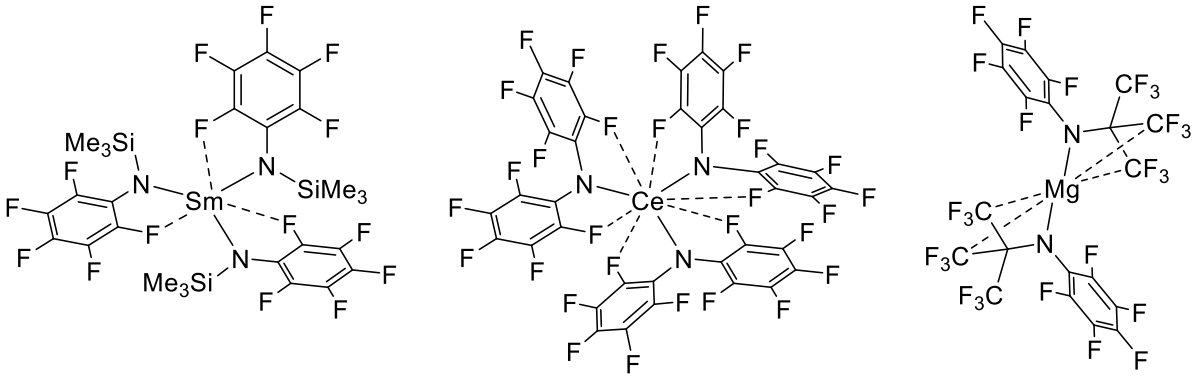


**Figure 2.** Selected examples of homoleptic fluorinated arylamido complexes.

One topical field of studies in main group chemistry aims at devising low-coordinate alkaline earth molecular (pre)catalysts that present an optimal compromise between stability and reactivity. Improving our understanding of the nature of the bonding, especially with respect to secondary interactions, is key in this purpose. We are presenting here the outcome of our investigations concerning the syntheses, structures and bonding patterns in calcium and barium complexes, including heteroleptic ones, supported by the perfluorinated arylamide $N(C_6F_5)_2^-$. Spectroscopic and crystallographic data are discussed in the light of complementary DFT computations and bond valence sum analysis.[17]

10.1002/chem.201901262

## Results and Discussion

*Synthesis of complexes*

Our investigations started with the attempted preparations of calcium-based starting materials devoid of coordinated Lewis bases. The homoleptic complex [Ca{N(C$_6$F$_5$)$_2$}$_2$] (**4**) was obtained in a non-optimised 82% yield by treatment of [Ca{N(SiMe$_3$)$_2$}$_2$]$_2$ with a stoichiometric amount of the perfluorinated arylamine HN(C$_6$F$_5$)$_2$[18] in toluene (Scheme 1). Complex **4**, the nuclearity of which could not be established, is only sparingly soluble in aliphatic and aromatic hydrocarbons; single crystals of **4** suitable for X-ray diffractometry could not be obtained in spite of multiple attempts. Layering a petroleum ether solution of [Ca{N(SiMe$_3$)$_2$}$_2$]$_2$ with a solution of HN(C$_6$F$_5$)$_2$ in this solvent also proved inadequate.[14b] On the other hand, **4** is soluble in ethers and colourless crystals of the diethyl ether adduct [Ca{N(C$_6$F$_5$)$_2$}$_2$.(Et$_2$O)$_2$] (**4'**) were grown upon recrystallisation from a diethyl ether solution.

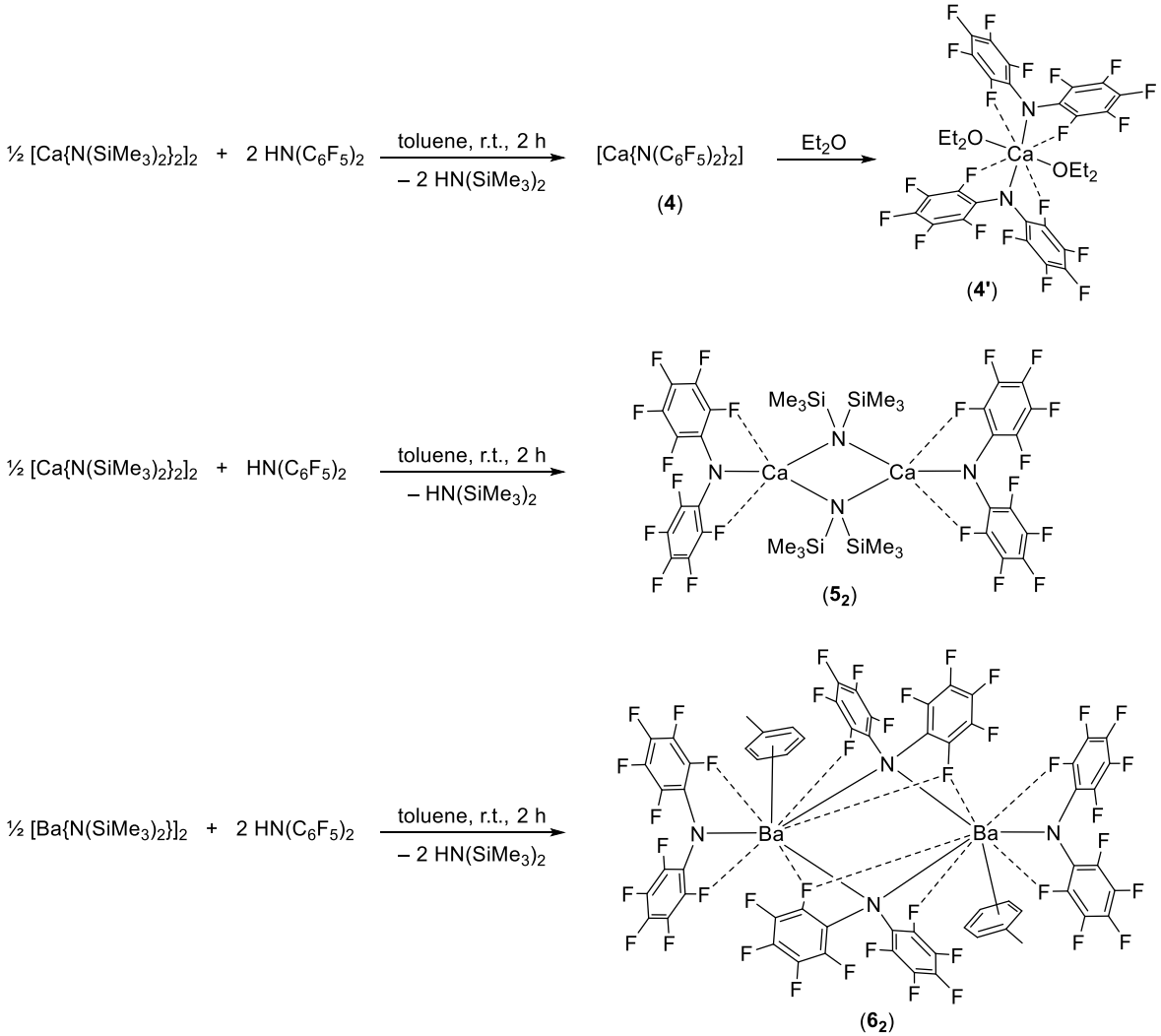


**Scheme 1.** Synthesis of fluoroarylamide-containing starting materials [Ca{N(C$_6$F$_5$)$_2$}$_2$] (**4**), [Ca{N(C$_6$F$_5$)$_2$}$_2$.(Et$_2$O)$_2$] (**4'**), [Ca{$\mu^2$-N(SiMe$_3$)$_2$}{N(C$_6$F$_5$)$_2$}]$_2$ (**5$_2$**) and [Ba{$\mu$-N(C$_6$F$_5$)$_2$}{N(C$_6$F$_5$)$_2$}.toluene]$_2$ (**6$_2$**), with representation of their molecular solid-state structures (structure for complex **4** unknown).

10.1002/chem.201901262

The $^{19}$F NMR spectrum of complex **4'** in benzene-$d_6$ at room temperature is characterised by three resonances: a doublet centred on δ –153.80 ppm for *o*-F atoms, and two overlapping triplets in the region δ –162.60 to –163.00 ppm for *m*- and *p*-F. Its $^{1}$H NMR spectrum solely indicates the presence of coordinated diethyl ether. By comparison, the $^{19}$F NMR spectrum of ether-free **4** in thf-$d_8$ exhibits three broad resonances at δ –159.45, –168.88 and –178.23 ppm integrating respectively for 8, 8 and 4F atoms. The heteroleptic dinuclear complex [Ca{μ$^2$-N(SiMe$_3$)$_2$}{N(C$_6$F$_5$)$_2$}]$_2$ (**5$_2$**) was synthesised by reacting [Ca{N(SiMe$_3$)$_2$}$_2$]$_2$ with two equiv of HN(C$_6$F$_5$)$_2$ in toluene. It was isolated in 64% yield as colourless crystals upon recrystallisation from a concentrated solution in 1,2-difluorobenzene, and its solid-state structure was established (vide infra). Its solubility in hydrocarbons, Et$_2$O and thf is high. The $^{1}$H NMR spectrum of **5$_2$** (benzene-$d_6$, 25 °C) expectedly features a single resonance, a singlet at δ 0.01 ppm. Three sharp and well separated resonances are detected in its $^{19}$F NMR spectrum, respectively for *o*-, *m*- and *p*-F atoms: a doublet at δ –156.14 ppm, and two triplets at δ –164.58 and –172.65 ppm. The high-field $^{19}$F chemical shifts observed in **5$_2$**, compared to those in the parent amine (δ –154.42, –163.19 and –163.48 for *o*-, *p*- and *m*-F atoms, respectively), are consistent with the accumulation of a negative charge on the $N_{amide}$ atom on passing from HN(C$_6$F$_5$)$_2$ to **5$_2$** where bonding is predominantly ionic.

To assess the possibility of combining the fluoroarylamine with a larger alkaline earth metal, the stoichiometric reaction of [Ba{N(SiMe$_3$)$_2$}$_2$]$_2$ with HN(C$_6$F$_5$)$_2$ afforded the dinuclear barium complex [Ba{μ-N(C$_6$F$_5$)$_2$}{N(C$_6$F$_5$)$_2$}.toluene]$_2$ (**6$_2$**). This complex is moderately soluble in petroleum ether and aromatic hydrocarbons. The presence of one coordinated toluene molecule per Ba$^{2+}$ (which could not be removed, even by heating under dynamic vacuum) was established by $^{1}$H and $^{13}$C{$^{1}$H} NMR in benzene-$d_6$ and by XRD analysis. Coordination of toluene testifies to the electrophilic nature of the Ba$^{2+}$ ions in complex **6$_2$**. Its $^{19}$F NMR spectrum recorded at 25 °C show broad resonances of expected intensities for *o*-, *m*- and *p*-F atoms centred on δ –157.66, –165.85 and –176.06 ppm, close to those of **5$_2$**.

The heteroleptic **5$_2$**, with its basic N(SiMe$_3$)$_2^-$ amide (*p*Ka = 25.8 in thf[19]), was used as a precursor to other heteroleptic species. NMR monitoring of the reaction of **5$_2$** with the β-diketimine {BDI$^{DiPP}$}H (2 equiv) in toluene-$d_8$ showed quantitative formation of the dinuclear [{BDI$^{DiPP}$}CaN(C$_6$F$_5$)$_2$]$_2$ (**7$_2$**) upon selective release of HN(SiMe$_3$)$_2$ (Scheme 2). The reaction subsequently performed on larger scales afforded the formally three-coordinate **7$_2$** as a colourless solid in reproducible 80-90% yields. Its $^{1}$H NMR spectrum recorded in toluene-$d_8$ showed the formation of a pure product, characterised notably by a singlet at δ 4.77 ppm diagnostic of the {BDI$^{DiPP}$}$^-$ backbone methine C*H* hydrogen atom, and the absence of residual N(SiMe$_3$)$_2^-$. The $^{19}$F NMR spectrum of the complex exhibits a doublet at δ –158.11 and two triplets at δ –164.85 and –175.62 ppm for *o*-, *m*- and *p*-F atoms, respectively. Complex **7$_2$** can be seen as the derivative of [{BDI$^{DiPP}$}CaN(SiMe$_3$)$_2$] (**3**).[8] It is more easily accessed than this latter complex and in greater yields, but the fluoroarylamide in **7$_2$** is less basic and less reactive than the N(SiMe$_3$)$_2^-$ residue in **3**. In a similar way to **7$_2$**, the dinuclear complex [{N^N$^{DiPP}$}CaN(C$_6$F$_5$)$_2$]$_2$ (**8$_2$**) was obtained near-quantitatively by reacting **5$_2$** with two equiv of the iminoaniline {N^N$^{DiPP}$}H. As for **7$_2$**, with which it shares comparable organisation in the solid state (*vide infra*), the $^{1}$H and $^{19}$F NMR spectra

10.1002/chem.201901262

of **8₂** recorded at 25 °C in toluene-$d_8$ confirms the presence of a single environment. Well-resolved diagnostic resonances are located at δ 7.92 ppm in the $^1$H spectrum for the C*H*=N hydrogen atom, and at δ –158.11, –164.78 and –175.95 ppm (for *o*-, *m*- and *p*-F atoms, respectively) in the $^{19}$F NMR spectrum. Complexes **7₂** and **8₂** are only moderately soluble in petroleum ethers and toluene.

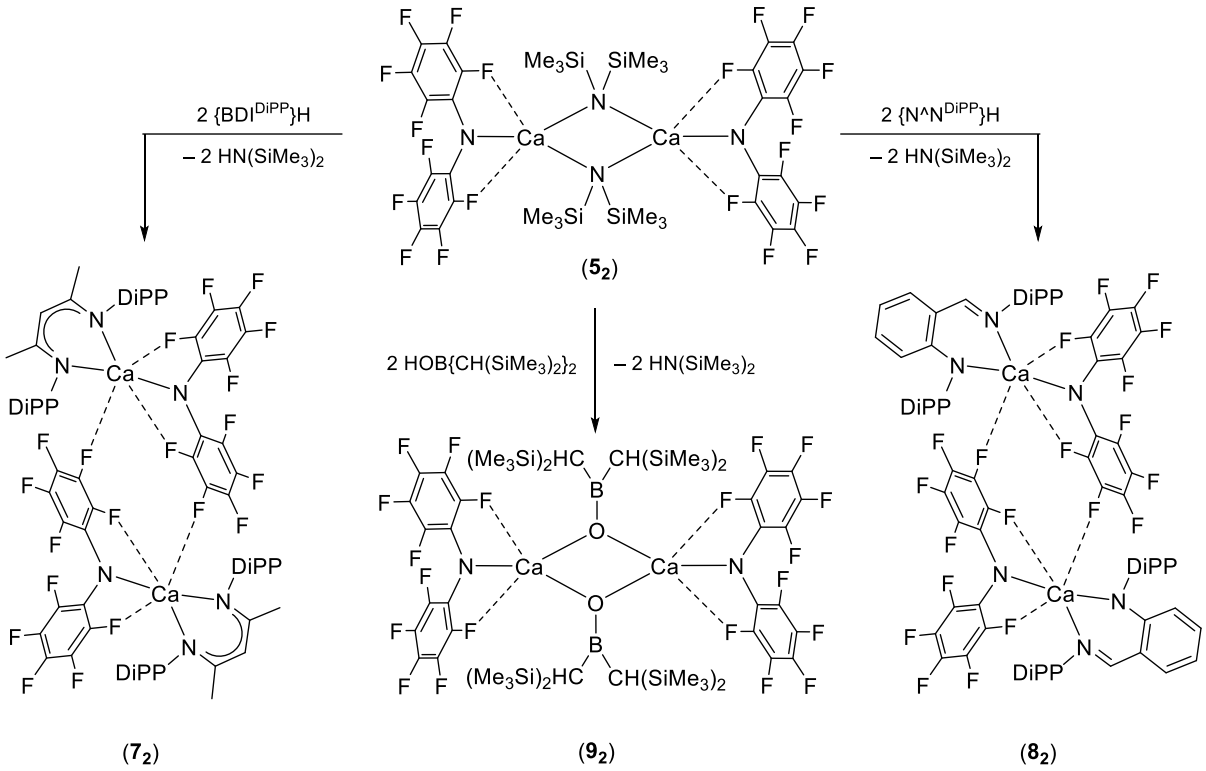


**Scheme 2.** Synthesis of fluoroarylamide-containing [{BDI$^{DiPP}$}CaN(C$_6$F$_5$)$_2$]$_2$ (**7₂**), [{N^N$^{DiPP}$}CaN(C$_6$F$_5$)$_2$]$_2$ (**8₂**), and [Ca{μ-OB(CH(SiMe$_3$)$_2$)$_2$}{N(C$_6$F$_5$)$_2$}]$_2$ (**9₂**), with representation of their molecular solid-state structures.

It has recently been established that boryloxides could yield barium complexes of the type [Ba(OBR$_2$)$_2$] with coordination numbers as low as two.[3d] In an attempt to extend this reactivity to calcium and combine it with fluoroarylamides, the colourless [Ca{μ-OB(CH(SiMe$_3$)$_2$)$_2$}{N(C$_6$F$_5$)$_2$}]$_2$ (**9₂**) was isolated in high yield following the stoichiometric reaction of **5₂** with the borinic acid HOB{CH(SiMe$_3$)$_2$}$_2$. Complex **9₂** is the first reported example of calcium boryloxide.[20] It is only mildly soluble in hydrocarbons, but dissolves upon heating. Its $^1$H NMR spectrum in benzene-$d_6$ is characterised by two sets of resonances of matching intensities for C*H*(SiMe$_3$)$_2$ and C*H*$_3$ hydrogens in non-equivalent boryloxides: one at δ 0.21 and 0.15 ppm, and the other at 0.20 and 0.05 ppm. The $^{19}$F NMR spectrum also exhibits two sets of equal intensities for *o*-, *m*- and *p*-F atoms: at δ –155.79 (d, 8F), –163.59 (t, 8F) and –173.47 (t, 4F) ppm for one, and at δ –158.73 (d, 8F), –164.74 (t, 8F) and –174.45 (t, 4F) ppm for the other. Typically for this boryloxide,[3d] a single resonance at δ 53.71 ppm is seen in the $^{11}$B NMR spectrum. This pattern agrees with the $C_2$-symmetry axis seen in the solid-state structure

10.1002/chem.201901262

of the complex, with two distinct pairs of $C_6F_5$ groups due to hindered rotation along the Ca–N axes, although an dynamic association-dissociation of the dimer in solution cannot be ruled out.

*Structural studies – X-ray diffraction crystallography*

The molecular solid-state structure of $[Ca\{N(C_6F_5)_2\}_2.(Et_2O)_2]$ (**4'**) determined by XRD analysis is depicted in Figure 3. The coordination sphere comprises two $N_{C6F5}$ and two $O_{ether}$ atoms, and the metal centre rests in a distorted tetrahedral environment. The Ca–$N_{C6F5}$ bond lengths in **4'** (2.370(1) and 2.380(1) Å) are substantially longer than the corresponding ones in the related bis(amido) complex $[Ca\{N(SiMe_3)_2\}_2.(thf)_2]_2$ (2.294(3) and 2.309(3) Å).[21] This reflects the greater electron withdrawing ability of the $N(C_6F_5)_2^-$ moiety and, as a result, the greater ionicity on the Ca–N bond in **4'**. The electrophilicity of the calcium atoms in **4'** is partly compensated by Ca–$O_{ether}$ bonds (2.340(1) and 2.342(1) Å) stronger than in $[Ca\{N(SiMe_3)_2\}_2.(thf)_2]_2$ (2.369(3) and 2.385(3) Å). In addition, further electronic density is provided to the metal by four Ca···F–C intramolecular interactions in the range 2.493(1)-3.074(1) Å. Considering that the accepted limit for Ca···F contacts is commonly set at 3.13 Å,[22] two of them, at 2.493(1) and 2.523(1), can be regarded as extremely strong. They for instance compare well with those found in an unusual homoleptic β-diketiminato calcium complex bearing $CF_3$ substituents in the backbone of the $\eta^1$-bonded ligands.[12a] These Ca···F–C interactions may also be a factor to the long Ca–$N_{C6F5}$ bond length.

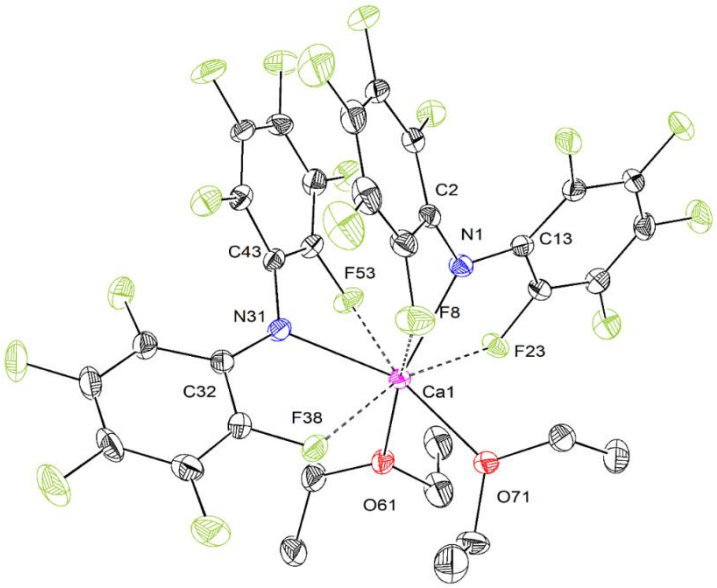


**Figure 3.** ORTEP representation of the molecular solid-state structure of $[Ca\{N(C_6F_5)_2\}_2.(Et_2O)_2]$ (**4'**). Ellipsoids at the 50% probability level, with only the main component of the disordered $Et_2O$ molecule. H atoms omitted for clarity. Ca···F interactions depicted in dashed bonds. Selected bond lengths (Å) and angles (deg): Ca1-O61 = 2.3402(12), Ca1-O71 = 2.3421(12), Ca1-N31 = 2.3705(14), Ca1-N1 = 2.3805(14), Ca1-F23 = 2.4935(10), Ca1-F38 = 2.5226(10), Ca1-F53 = 2.7713(11), Ca1-F8 = 3.0740(12); O61-Ca1-O71 = 87.71(4), O61-Ca1-N31 = 100.65(5), O71-Ca1-N31 = 144.30(5), O61-Ca1-N1 = 143.24(5), O71-Ca1-N1 = 98.38(5), N31-Ca1-N1 = 95.23(5).

10.1002/chem.201901262

The solid-state structure of [Ca{μ²-N(SiMe$_3$)$_2$}{N(C$_6$F$_5$)$_2$}]$_2$ (**5$_2$**), with its crystallographic $C_1$ symmetry, shows a dinuclear arrangement (Figure 4). The more electron-rich hexamethyldisilazide groups N(SiMe$_3$)$_2^-$ occupy the bridging positions. The corresponding Ca–N$_{HMDS}$ bond lengths, in the range 2.404(2)-2.439(2) Å, are shorter than their homologues in [Ca{μ²-N(SiMe$_3$)$_2$}{N(SiMe$_3$)$_2$}]$_2$, where they are found between 2.431(7) and 2.521(7) Å.[23] The distances to the terminal $N_{C6F5}$ groups, at 2.385(2) and 2.383(2) Å, are comparable to those in **4'**. Taking the three *N* atoms into account, each calcium in **5$_2$** lies in a perfect trigonal planar geometry ($\Sigma_\theta$(Ca1) = 359.95 ° and $\Sigma_\theta$(Ca2) = 359.90 °). Besides, each also engages in a strong Ca···F–C interaction, as indicated by short Ca1–F43 and Ca2–F62 distances (2.423(2) and 2.456(2) Å). Complex **5$_2$** is a rare example of charge-neutral three-coordinate calcium complex free of coordinated solvent; other representative examples include [Ca{N(SiMe$_3$)$_2$}$_2$]$_2$ and [{BDI$^{DiPP}$}CaN(SiMe$_3$)$_2$] (**3**) already mentioned,[6e,8,23] as well as [Ca(O-*t*Bu$_2$-2,6-C$_6$H$_3$)$_2$]$_2$,[24] the *N*-heterocyclic carbene adducts [Ca{N(SiMe$_3$)$_2$}$_2$.NHC$^{aryl}$] (aryl = mesityl or 2,6-*i*Pr$_2$C$_6$H$_3$),[25] and the imine adduct [Ca{N(SiMe$_3$)$_2$}$_2$.PhCH=N*t*Bu].[26,27]

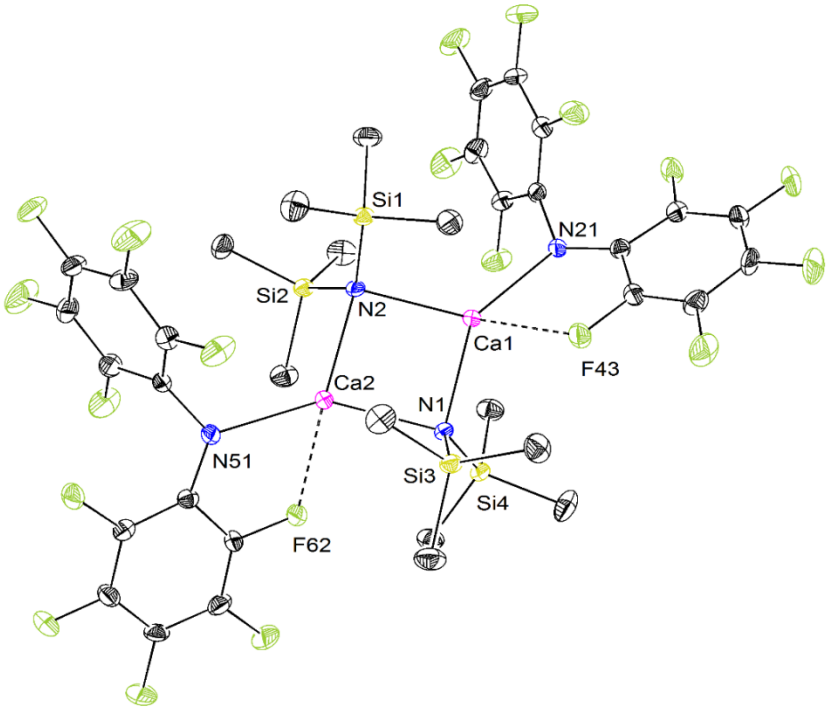


**Figure 4.** ORTEP representation of the molecular solid-state structure of [Ca{μ²-N(SiMe$_3$)$_2$}{N(C$_6$F$_5$)$_2$}]$_2$ (**5$_2$**). Only one of the two independent but similar molecules in the asymmetric unit represented. Ellipsoids at the 50% probability level. H atoms omitted for clarity. Ca···F interactions depicted in dashed bonds. Selected bond lengths (Å) and angles (deg): Ca1-N21 = 2.385(2), Ca1-N2 = 2.404(2), Ca1-F43 = 2.4227(18), Ca1-N1 = 2.433(2), Ca2-N51 = 2.383(2), Ca2-N2 = 2.411(2), Ca2-N1 = 2.439(2), Ca2-F62 = 2.4560(18); N21-Ca1-N2 = 125.47(8), N21-Ca1-N1 = 145.63(8), N2-Ca1-N1 = 88.85(8), F43-Ca1-N1 = 85.00(7), N51-Ca2-N2 = 125.06(8), N51-Ca2-N1 = 145.99(8), N2-Ca2-N1 = 88.55(8).

10.1002/chem.201901262

The centrosymmetric barium complex [Ba{μ-N($C_6F_5$)$_2$}{N($C_6F_5$)$_2$}.toluene]$_2$ (**6$_2$**) is dinuclear (Figure 5). The Ba–N interatomic distances to terminal and bridging *N*-atoms, respectively of 2.740(3) and 2.871(4)-2.951(3) Å, are longer than in the related [Ba{μ-N($SiMe_3$)$_2$}{N($SiMe_3$)$_2$}]$_2$ (2.576(3) and 2.798(3)-2.846(4) Å).[28] This again results from lower electron availability in N($C_6F_5$)$_2^-$ and greater ionic bonding in **6$_2$** due to the presence of very electron-withdrawing substituents on the *N*-atoms. In addition to the fluoroarylamides, the coordination sphere of each $Ba^{2+}$ cation in **6$_2$** is completed by a capping $\eta^6$-coordinated toluene molecule, with a Ba-centroid distance of 3.065 Å and corresponding Ba-$C_{toluene}$ distances between 3.287(5) and 3.436(6) Å. Coordinative unsaturation is further relieved by five close Ba···F–C contacts, with Ba–F distances in the range 2.825(2)-3.014(3) Å. The formation of a dinuclear species, the high number of Ba···F–C contacts (e.g. compared to **4'** and **5$_2$**) and additional coordination of toluene molecules are seen as the reflection of the great electrophilicity of the $Ba^{2+}$ cations in **6$_2$**. Ba···$C_\pi$ interactions are common in complexes of barium, a metal softer than calcium.[9,29] Ba···F–C interactions are known to stabilise electron-deficient barium complexes. The intramolecular Ba–F distances are for instance of 2.871(2) and 2.901(3) Å in [(thf)$_2$Ba{N(H)-2,6-$F_2$-$C_6H_3$}]$_\infty$,[12b] while they range from 2.918(2) to 2.992(3) Å in discrete monocationic complexes bearing multidentate aminoether-fluoroalkoxides.[4b,30]

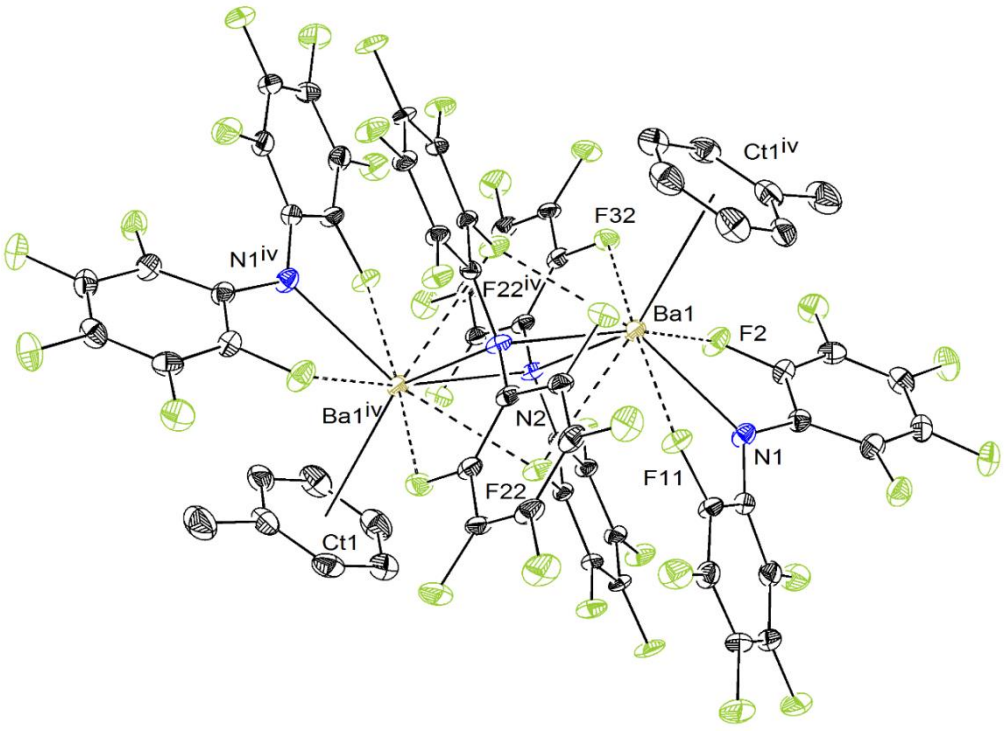


**Figure 5.** ORTEP representation of the molecular solid-state structure of [Ba{μ-N($C_6F_5$)$_2$}{N($C_6F_5$)$_2$}.toluene]$_2$ (**6$_2$**). Ellipsoids at the 50% probability level. H atoms omitted for clarity. Ba···F interactions depicted in dashed bonds. Selected bond lengths (Å): Ba1-N1 = 2.740(3), Ba1-F11 = 2.825(2), Ba1-F32 = 2.832(2), Ba1-N2 = 2.871(4), Ba1-F2 = 2.910(3), Ba1-F22$^{iv}$ = 2.923(3), Ba1-N2$^{iv}$ = 2.951(3), Ba-F22 = 3.014(3).

10.1002/chem.201901262

The solid-state structure of [{BDI$^{DiPP}$}CaN($C_6F_5$)$_2$]$_2$ (**7$_2$**) is displayed in Figure 6. It shows the complex to exist as a dimer in the solid state through the presence of two *intermolecular* Ca···F–C contacts with *m*-F atoms carried by a neighbouring $C_6F_5$ moieties. The dimer possesses a crystallographic $C_2$ symmetry axis that goes through the two calcium atoms. Compound **7$_2$**, where the metal centres are formally three-coordinate, is most closely related to [{BDI$^{DiPP}$}CaN($SiMe_3$)$_2$] (**3**): this complex, with three-coordinate metal centres, forms tetramers in the solid phase through intermolecular Ca···$H_3C$ interactions, and also displays intramolecular Ca···$H_3C$ contacts.[8] The Ca–N interatomic distances to $N_{BDIiPP}$-atoms in the bidentate ligand in **7$_2$** (2.306(2) and 2.346(2) Å) match those in **3** (2.323(3) and 2.331(3) Å). On the other hand, the Ca–$N_{C6F5}$ bond length in **7$_2$** is noticeably longer than the corresponding Ca–$N_{HMDS}$ one in **3** (2.388(2) vs 2.299(3) Å), showing that the more basic and electron-rich amide induces a tighter bond with calcium. Albeit weaker than in **4'** and **5$_2$**, the intramolecular (2.556(1), and 2.712(2) Å) and intermolecular (2.532(1) Å) Ca···F–C interactions in **7$_2$** remain on the whole particularly strong in regard of those found in many other calcium complexes.[12] The dinuclear configuration is held together solely through the intermolecular Ca···F–C contacts. The two $C_6F_5$ groups located between the two $Ca^{+2}$ ions are parallel, but this is due to the symmetry in **7$_2$**; there is no substantial π-stacking interaction between them, as they are in offset positions.

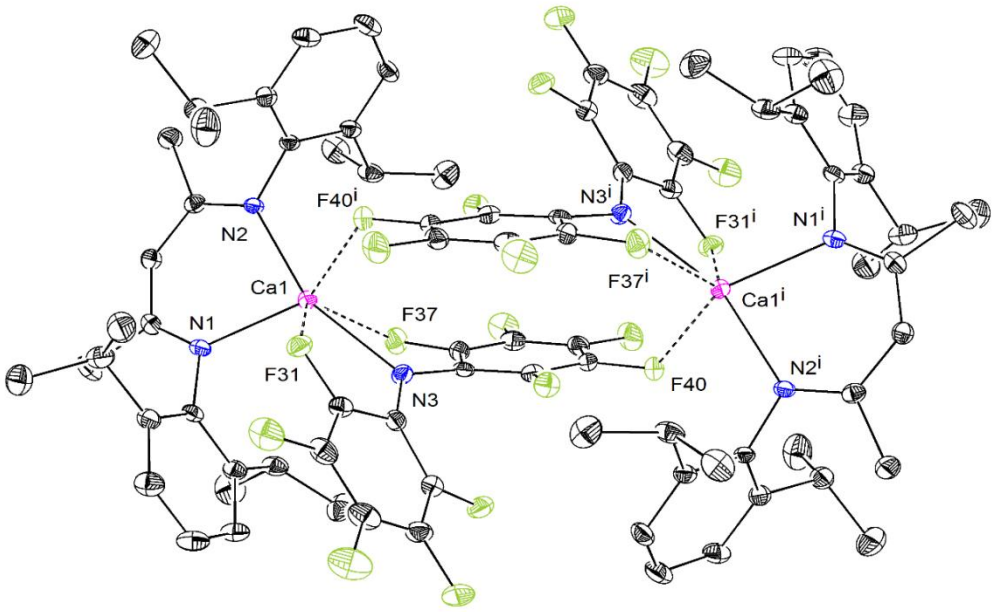


**Figure 6.** ORTEP representation of the molecular solid-state structure of [{BDI$^{DiPP}$}CaN($C_6F_5$)$_2$]$_2$ (**7$_2$**). Ellipsoids at the 50% probability level. H atoms and non-interacting benzene molecule omitted for clarity. Ca···F interactions depicted in dashed bonds. Selected bond lengths (Å): Ca1-N1 = 2.3066(19), Ca1-N2 = 2.3465(18), Ca1-N3 = 2.3880(19), Ca1-F40$^i$ = 2.5325(15), Ca1-F31 = 2.5559(15), Ca1-F37 = 2.7120(17).

10.1002/chem.201901262

Perhaps unsurprisingly on account of the similarities of their ligand backbones, the molecular structure of [{N^N$^{DiPP}$}CaN($C_6F_5$)$_2$]$_2$ (**8$_2$**) is very similar to that of **7$_2$**; it is given in the Supporting Information, without further discussion here.

The heteroleptic boryloxide/fluoroarylamide complex [Ca{μ-OB(CH($SiMe_3$)$_2$)$_2$}{N($C_6F_5$)$_2$}]$_2$ (**9$_2$**) is dinuclear in the solid state, with formally three-coordinate calcium centres surrounded by boryloxides in bridging positions and amides in terminal ones (Figure 7). This is the opposite situation of that in the barium complex [Ba{μ$^2$-N($SiMe_3$)$_2$}(OB{CH($SiMe_3$)$_2$}$_2$)]$_2$, where N($SiMe_3$)$_2^-$ amides, more electron-rich than N($C_6F_5$)$_2^-$, occupy the bridging positions.[3d] Hence, the overall electron availability and donating ability in these monoanionic ligands increases with N($C_6F_5$)$_2^-$ < OB{CH($SiMe_3$)$_2$}$_2^-$ < N($SiMe_3$)$_2^-$. Delocalisation of *N*-electrons into antibonding σ(Si–C*) orbitals that takes place in N($SiMe_3$)$_2^-$ is of limited effect compared to partial delocalisation of *O*-electrons into the empty $p_z$ orbital at boron in the boryloxide, while the presence of two strongly electron-withdrawing groups in N($C_6F_5$)$_2^-$ bears the strongest effect on electron-sharing properties.

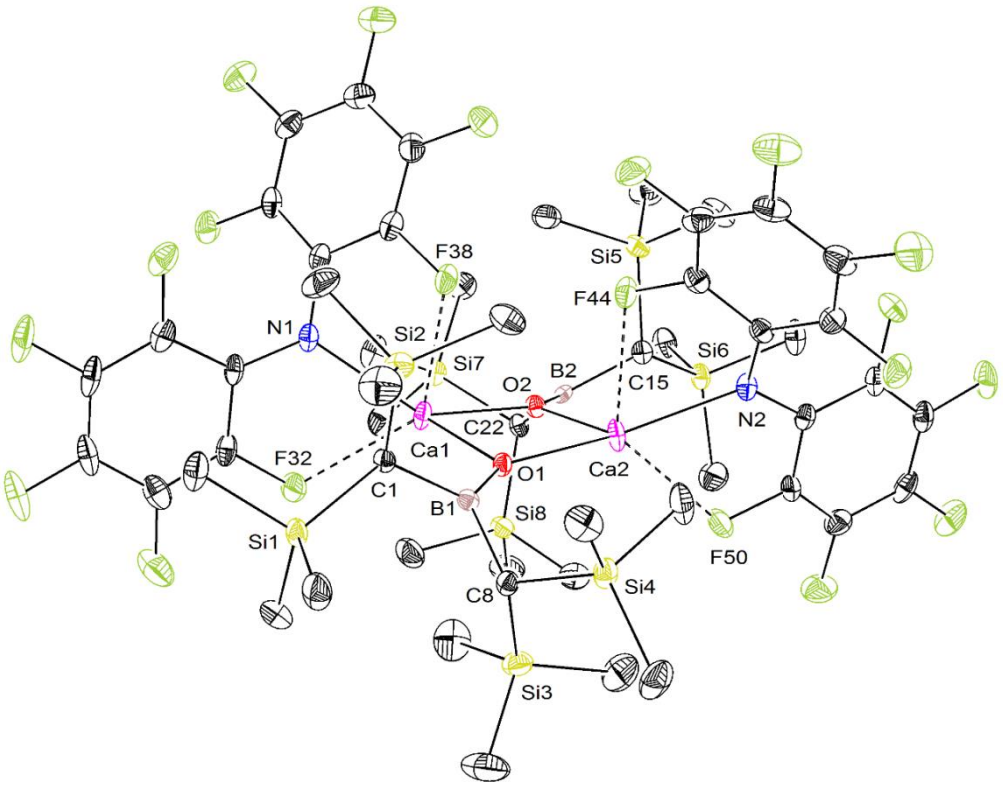


**Figure 7.** ORTEP representation of the molecular solid-state structure of [Ca{μ-OB(CH($SiMe_3$)$_2$)$_2$}{N($C_6F_5$)$_2$}]$_2$ (**9$_2$**). Ellipsoids at the 50% probability level. H atoms omitted for clarity. Ca···F interactions depicted in dashed bonds. Selected bond lengths (Å): Ca1-O2 = 2.269(2), Ca1-O1 = 2.271(2), Ca1-N1 = 2.370(3), Ca1-F32 = 2.544(2), Ca1-F38 = 2.597(2), Ca2-O1 = 2.243(2), Ca2-O2 = 2.259(2), Ca2-N2 = 2.356(3), Ca2-F50 = 2.498(2), Ca2-F44 = 2.553(2); O2-Ca1-O1 = 82.58(8), O2-Ca1-N1 = 138.45(9), O1-Ca1-N1 = 124.32(10), O1-Ca2-O2 = 83.40(8), O1-Ca2-N2 = 143.23(10), O2-Ca2-N2 = 126.74(9).

By contrast with **5₂**, where each three-coordinate $Ca^{2+}$ is in a trigonal planar geometry, the arrangement around Ca1 and Ca2 in **9₂** is irregular ($\Sigma_\theta$(Ca1) = 345.35 ° and $\Sigma_\theta$(Ca2) = 353.37 °, taking *N* and *O* atoms into account). This may reflect high steric congestion around the metals, or can also be the consequence of two Ca···F–C interactions per metal, as opposed to one in **5₂**. The strength of the various Ca···F–C interactions in **9₂**, with interatomic distances of 2.544(2) and 2.597(2) for Ca1 and 2.498(2) and 2.553(2) for Ca2, appears to be weaker than in **5₂**. The geometry around the boron, oxygen and nitrogen atoms approaches perfect trigonal planarity in all cases ($\Sigma_\theta$(B1) = 359.90 ° and $\Sigma_\theta$(B2) = 359.90 °; $\Sigma_\theta$(O1) = 359.96 ° and $\Sigma_\theta$(O2) = 359.96 °; $\Sigma_\theta$(N1) = 359.80 ° and $\Sigma_\theta$(N2) = 359.90 °).

*Bond valence sum analysis*

The contribution of Ca···F–C secondary interactions towards the coordination sphere of the $Ca^{2+}$ ions in our low-coordinate [Ca]-N($C_6F_5$)$_2$ complexes was gauged using bond valence sum (BVS) analysis. This empirical treatment, pioneered by Brown and further developed by O'Keefe and Brese,[17] makes use of interatomic distances measured by single-crystal X-ray diffraction to evaluate the relative contributions of each neighbouring atom towards the coordination sphere of a given metallic centre. It has been applied in recent years to analyse the bonding patterns of a variety of *s*-block complexes, in particular to evaluate the role of non-covalent interactions.[12d,31] For each complex, bond valences (ν) were calculated using eq 1, with experimental bond lengths $d_{Ca\text{-}X}$ and tabulated (empirical) bond valence parameters $R_{Ca–X}$:

$$\nu = \exp[(R_{Ca–X} - d_{Ca–X})/B] \quad (1)$$

in which X = O, F, N; B = 0.37; $R_{Ca–O}$ = 1.967, $R_{Ca–F}$ = 1.842 and $R_{Ca–N}$ = 2.140.[17] The bond valence value, ν, provides a quantitative appraisal of the contributions of secondary Ca···F–C interactions to the global coordination sphere of each $Ca^{2+}$ cation. The calculated sums of bond valence values ($\Sigma\nu_{Ca–X}$) for X = N/F/O) for each $Ca^{2+}$ in the calcium complexes **4'**, **5₂**, **7₂** and **9₂** are collated in Table 1. As anticipated for a divalent cation, the values approach 2, although the deviations observed in **5₂** and **9₂** may suggest that BVS analysis is not ideally suited to these very coordinatively unsaturated species.

Qualitative analysis of the data indicates that Ca···F–C interactions contribute to around 15% of the total bonding pattern, and culminate in the value of 20% estimated for complex **4'**. The remaining of the coordination sphere is filled out by Ca–N and, where relevant, Ca–O bonds. In the dinuclear complexes in which the two $Ca^{2+}$ centres are not identical (that is, **5₂** and **9₂**), the bonding patterns remain very comparable around the two cations. The contributions of Ca···F–C interactions to the bonding in **4'**, **5₂**, **7₂** and **9₂** outclass that established for a dinuclear complex [{$RO^F$}CaN($SiMe_3$)$_2$]$_2$ where each five-coordinate $Ca^{2+}$ was surrounded by an $\eta^3$-coordinated aminoether-fluoroalkoxide {$RO^F$}$^-$, and in which a single Ca···F–C contact counted for ca. 4% of the coordination sphere around each ion.[12d] This translates the growing importance of secondary interactions as the coordination number decreases.

10.1002/chem.201901262

**Table 1.** Bond valence sum analysis for the calcium complexes **4'**, **5₂**, **7₂** and **9₂**

| **Complex** | | | $d_{Ca-N}$ [a] | $d_{Ca-F}$ [a] | $d_{Ca-O}$ [a] | $v_{Ca-N}$ [b] | $v_{Ca-F}$ [b] | $v_{Ca-O}$ [b] | $\Sigma(v_{Ca-X})$ |
|---|---|---|---|---|---|---|---|---|---|
| $[Ca\{N(C_6F_5)_2\}_2.(Et_2O)_2]$ (**4'**) | Ca1 | | 2.380 | 2.493 | 2.340 | 0.52 | 0.17 | 0.36 | |
| One 4-coordinate Ca atom | | | 2.370 | 2.523 | 2.342 | 0.54 | 0.16 | 0.36 | |
| | | | - | 2.771 | - | - | 0.08 | - | |
| | | | - | 3.074 | - | - | 0.04 | - | |
| | | $\Sigma(v_{Ca1-X})$ | | | | 1.06 | 0.45 | 0.73 | 2.24 |
| | | $\%(v_{Ca1-X})$ | | | | 47 | 20 | 33 | 100% |
| $[Ca\{\mu^2\text{-}N(SiMe_3)_2\}\{N(C_6F_5)_2\}]_2$ (**5₂**) | Ca1 | | 2.433 | 2.423 | - | 0.45 | 0.21 | - | |
| Two distinct 3-coordinate Ca atoms | | | 2.404 | - | - | 0.49 | - | - | |
| | | | 2.385 | - | - | 0.52 | - | - | |
| | | $\Sigma(v_{Ca1-X})$ | | | | 1.46 | 0.21 | - | 1.67 |
| | | $\%(v_{Ca1-X})$ | | | | 87 | 13 | - | 100 |
| | Ca2 | | 2.439 | 2.456 | - | 0.45 | 0.19 | - | |
| | | | 2.411 | - | - | 0.48 | - | - | |
| | | | 2.383 | - | - | 0.52 | - | - | |
| | | $\Sigma(v_{Ca2-X})$ | | | | 1.44 | 0.19 | - | 1.63 |
| | | $\%(v_{Ca2-X})$ | | | | 88 | 12 | - | 100 |
| $[\{BDI^{DiPP}\}CaN(C_6F_5)_2]_2$ (**7₂**) | Ca1 | | 2.307 | 2.532 | - | 0.64 | 0.15 | - | |
| Two identical 3-coordinate Ca atoms | | | 2.346 | 2.556 | - | 0.57 | 0.14 | - | |
| | | | 2.388 | 2.712 | - | 0.51 | 0.09 | - | |
| | | $\Sigma(v_{Ca1-X})$ | | | | 1.72 | 0.39 | - | 2.11 |
| | | $\%(v_{Ca1-X})$ | | | | 81 | 19 | - | 100 |
| $[Ca\{\mu\text{-}OB(CH(SiMe_3)_2)_2\}\{N(C_6F_5)_2\}]_2$ (**9₂**) | Ca1 | | 2.370 | 2.544 | 2.271 | 0.54 | 0.15 | 0.44 | |
| Two distinct 3-coordinate Ca atoms | | | - | 2.597 | 2.269 | - | 0.13 | 0.44 | |
| | | $\Sigma(v_{Ca1-X})$ | | | | 0.54 | 0.28 | 0.88 | 1.70 |
| | | $\%(v_{Ca1-X})$ | | | | 32 | 16 | 52 | 100 |
| | Ca2 | | 2.356 | 2.498 | 2.243 | 0.56 | 0.17 | 0.47 | |
| | | | - | 2.553 | 2.259 | - | 0.15 | 0.45 | |
| | | $\Sigma(v_{Ca2-X})$ | | | | 0.56 | 0.32 | 0.93 | 1.81 |
| | | $\%(v_{Ca2-X})$ | 2.356 | | | 31 | 18 | 51 | 100 |

[a] Measured interatomic distances to X = N, F or O atoms, given in Å; see Figures 3, 4, 6 and 7 for detail. [b] Bond valence contribution for atom X. [c] Sum of all contributions for the different atoms: X = N, F and O.

It can also be seen from Table 1 that the relative contributions to the bonding pattern around $Ca^{2+}$ is directly proportional to the number of Ca···F–C contacts detected in the solid state. Although caution must be applied in the appreciation of quantitative BVS analysis with these electrophilic complexes, there can be little doubt that Ca···F–C interactions bear a great influence in their overall stability. The structural data and BVS analysis for these compounds can be added to the growing body of evidences that testifies to the significance of secondary interactions in the coordination chemistry of *s*-block metals.[1,9]

*Bonding analysis by DFT calculations*

DFT calculations were performed on series of model systems at the PBE0/Def2-TZVP and PBE0/Def2-TZVP-D3 levels (see Computational details in the SI) to shed some light on the nature and strength of the Ae···F–C bonding in our complexes. Since, in these compounds, both Ae and F belong to the same molecule, one might have to consider the potential role of the pinch intramolecular effect that could force the two atoms to get close to each other. In a first approach, we ruled out this possibility by investigating bi-molecular systems, i.e. the interaction between one F-containing molecule or ion, namely $C_6H_5F$, $CH_3F$ and $F^-$, and a simplified calcium complex. Since most of the molecular structures described above exhibit an $Ae^{2+}$ ion in a trigonal planar coordination mode (not considering the Ae···F–C interactions), the model complex chosen for this initial study was the simple [{NH(CH)$_3$NH}Ca(NH$_2$)] (***A***). The optimised geometries of the three ***A***($C_6H_5F$), ***A***($CH_3F$) and ***A***$F^-$ bimolecular systems are shown in Figure 8. Optimisations were performed with and without considering the 3-parameter Grimme's empirical corrections (D3)[32] for dispersion forces. Such corrections are expected to take satisfyingly into account the van der Waals component of the Ca···F bonding. The Ca–F distances obtained with and without D3 corrections are reported at the top of Figure 8 in black and blue colours, respectively. A weak shortening of the Ca–F distances (lower than 1%) occurs when introducing dispersion forces, indicating that van der Waals bonding does not play a crucial role in the interaction. The Ca–F distance is only slightly shortened when going from ***A***($C_6H_5F$) to ***A***($CH_3F$) and Ca remains in an approximate planar $CaN_3$ coordination. The ***A***$F^-$ structure is different, with a very short Ca–F distance (2.09 Å) and a pyramidalised ($sp^3$) Ca atom. Clearly, ***A***$F^-$ exhibits strong Ca···F bonding.

A more detailed understanding of the nature of the Ca···F(–C) bonding in the above series is obtained by an energy decomposition analysis (EDA) of the interaction between two fragments, according to the Morokuma-Ziegler procedure.[33] The decomposition of the total bonding energy (TBE) between ***A*** and the $C_6H_5F$, $CH_3F$ and $F^-$ fragments in the three optimised systems of Fig. 8 is provided in Table 2 (D3 corrections considered). TBE is expressed as the sum of four components, the Pauli repulsion ($E_{Pauli}$), the electrostatic interaction energy ($E_{elstat}$), the orbital interaction energy ($E_{orb}$) and the component associated with the dispersion forces ($E_{disp}$). Unsurprisingly, $E_{Pauli}$ increases with a decrease of the Ca···F–C separation. It is overbalanced by the three other stabilizing components, of which $E_{elstat}$

prevails, indicating predominance of ionic bonding. In ***A***($C_6H_5F$), the $E_{orb}$ component is about half of $E_{elstat}$, indicating weak, although non-negligible, covalent interactions. Consistently with the above discussion on bond distances, the $E_{disp}$ contribution is minor, corroborating weak van der Waal interactions. While the EDA analysis of ***A***($CH_3F$) provides rather similar values and conclusions as those for ***A***($C_6H_5F$), different results were obtained for ***A***$F^-$. Clearly, this other model contains a real and strong Ca–F single bond of ionocovalent nature (note the significant $E_{orb}$ component), whereas in the two other models, the Ca···F–C interaction is about six-fold weaker.

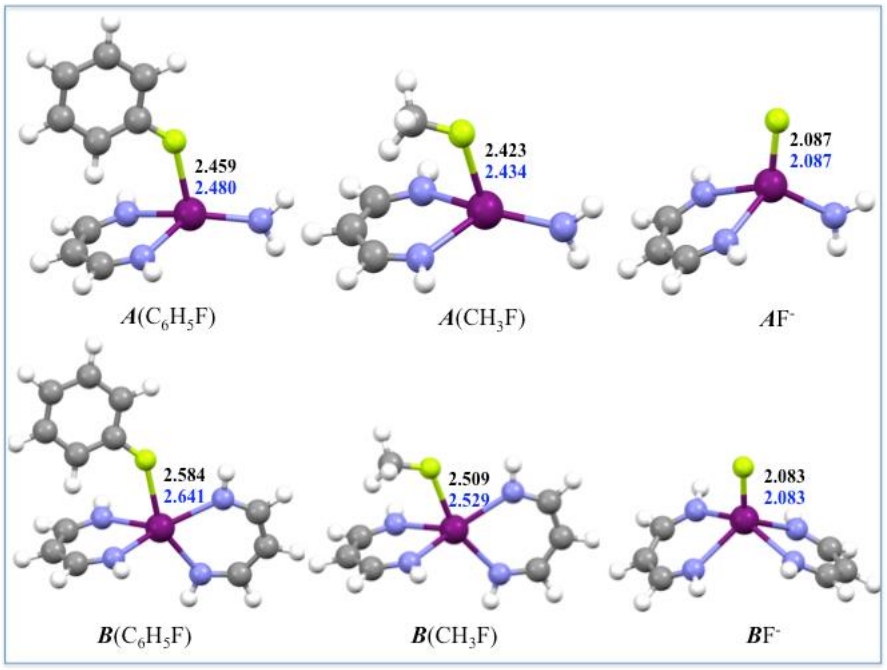


**Figure 8**. Optimised geometries of the ***A***($C_6H_5F$), ***A***($CH_3F$), ***A***$F^-$, ***B***($C_6H_5F$), ***B***($CH_3F$) and ***B***$F^-$ models. Interatomic distances are given in Å; in black, with D3 corrections; in blue, without D3 corrections.

**Table 2.** Morokuma-Ziegler energy decomposition analysis in the model compounds **7'$_2$** and those derived from [{$NH(CH)_3NH$}$Ca(NH_2)$] (= ***A***) and [{$NH(CH)_3NH$}$_2$Ca] (= ***B***). [a]

| | ***A***($C_6H_5F$) | ***A***($CH_3F$) | ***A***$F^-$ | **7'$_2$** | ***A***($CH_4$) | ***A***($C_6H_6$) | ***A***($C_2H_4$) | ***B***($C_6H_5F$) | ***B***($CH_3F$) | ***B***$F^-$ |
|---|---|---|---|---|---|---|---|---|---|---|
| $E_{Pauli}$ | 0.42 | 0.50 | 2.14 | 0.98 | 0.29 | 0.48 | 0.52 | 0.39 | 0.47 | 2.16 |
| $E_{elstat}$ | –0.53 | –0.71 | –4.46 | –0.95 | –0.24 | –0.53 | –0.54 | –0.44 | –0.61 | –4.22 |
| $E_{orb}$ | –0.28 | –0.28 | –1.31 | –0.62 | –0.19 | –0.41 | –0.27 | –0.21 | –0.22 | –1.43 |
| $E_{disp}$ | –0.15 | –0.11 | –0.02 | –0.80 | –0.09 | –0.21 | –0.11 | –0.17 | –0.11 | –0.02 |
| TBE [b] | –0.55 | –0.60 | –3.65 | –1.39 | –0.24 | –0.66 | –0.43 | –0.43 | –0.48 | –3.51 |

[a] all values in eV. [b] Total bonding energy = $E_{Pauli} + E_{elstat} + E_{orb} + E_{disp}$.

The weak Ca···F–C covalent contribution in ***A***($C_6H_5F$) and ***A***($CH_3F$) is in line with the natural atomic orbital (NAO) population analysis. In the two models, the computed F→Ca charge transfer is virtually nil (lower than $10^{-2}$), whereas it is 0.07 in *A*$F^-$. Surprisingly, the fluorine charge in ***A***($C_6H_5F$) and ***A***($CH_3F$) (–0.36 and –0.40, respectively) is more negative than in the free $C_6H_5F$ and $CH_3F$ ligands

(–0.31 and –0.35, respectively). This is diagnostic of strong electrostatic interaction with Ca, which attracts electron density towards the fluorine, but without any significant F→Ca electron transfer due to the poor bond covalence.

Since in the solid state, compounds **7₂** and **8₂** are dimers of mononuclear three-coordinate Ca complexes paired through intermolecular Ca···F–C contacts, an EDA analysis of the interaction between the two monomers was also carried out. Compound **7₂** was slightly simplified by replacing its Dipp and methyl substituents by hydrogen atoms. The geometry of this model (**7'₂**) was fully optimised at the PBE0/Def2-TZVP-D3 level. It showed the presence of Ca···F–C intermolecular contacts with interatomic distances of 2.584 and 2.612 Å, whereas the intramolecular contact was 2.581 Å. The EDA data obtained for **7'₂** on the basis of two monomeric fragments are given in Table 2. Considering that there are four inter-monomer Ca···F–C contacts (but somewhat longer that in *A*($C_5H_5F$), see below and Table 3), and that other van de Waals contacts are also present (see the structure of **7₂** in Fig. 6), the interaction energy component of **7'₂** are fully consistent with that of the simple *A*($C_5H_5F$) model.

In the above-computed models, the calcium atom lies in an approximate trigonal planar geometry (except for ***A***$F^-$), thus having its accepting $3p_z$ orbital essentially pointing in the direction of the electron-rich fluorine atom. A point of interest is the importance of the (weak) covalent interaction when calcium is tetravalent, being in a distorted $sp^3$ hybridisation. To probe this aspect, three other models, namely ***B***($C_6H_5F$), ***B***($CH_3F$) and ***B***$F^-$ in which ***B*** is [{$NH(CH)_3NH$}$_2$Ca], were investigated. Their optimised geometries are shown in Figure 8 (bottom). On going from ***A*** to ***B*** systems, only a small lengthening of the Ca–F distances is noticed. Consistently, the EDA components of the various ***B*** models do not differ much from that of their ***A*** homologues. Thus, on switching from a $sp^2$ to a $sp^3$ calcium, its (moderate) accepting properties do not vary significantly, owing to its propensity for hypervalence. In the weakly bonded ***B***($C_6H_5F$) and ***B***($CH_3F$), the Ca-centred $CaN_4$ polyhedron maintains its distorted tetrahedral configuration. On the other hand, ***B***$F^-$ is structurally different from the two other ***B*** systems. With a real Ca–F single bond, Ca is in a hypercoordinated square-pyramidal environment in ***B***$F^-$.

The real intramolecular Ca···F–C interactions detected in the molecular structures of compounds **4'**, **5₂**, **7₂** and **9₂** are also suitably reproduced in the structure of the fully optimised molecules (dispersion forces included, Table 3). There is however one noticeable exception, namely the long Ca···F–C contact (3.074(12) Å) observed in the X-ray structure of **4'**, which is found to be much shorter (2.769 Å) in the nearly $C_2$-symmetric optimised structure. This discrepancy is attributed to the packing interactions in the solid state, which distort the molecule away from ideal $C_2$ symmetry. The smaller deviation of ca. 0.10 Å found for the inter-monomer contact in **7₂** is likely the result of the simplification made on going from **7₂** to the less crowed **7'₂** model. As a whole, these data are fully consistent with those obtained in our simple intermolecular models, providing full confidence on the validity of our analysis of the bonding scenario. The above-observed electro-attracting effect of calcium onto the fluorine without any noticeable F→Ca electron transfer is also present in these compounds. With a NAO charge comprised

between –0.30 and –0.38, all fluorine atoms involved in Ca···F–C bonding are more negatively polarised that the other fluorine atoms, the NAO charge of which being comprised between –0.27 and –0.29. The major ionic character of the interaction is also consistent with the large positive charge computed for calcium in these compounds (between +1.81 and +1.84).

**Table 3.** Comparison of experimental and computed Ca···F–C interatomic distances for the calcium complexes **4'**, $\mathbf{5_2}$, $\mathbf{7_2}$ and $\mathbf{9_2}$

| **Complex** | | $d_{Ca–F}$ (XRD) [a] | $d_{Ca–F}$ (DFT) [b] |
|---|---|---|---|
| $[Ca\{N(C_6F_5)_2\}_2.(Et_2O)_2]$ (**4'**)<br>One 4-coordinate Ca atom | Ca1 | 2.4935<br>2.5226<br>2.7713<br>3.0740 | 2.553<br>2.552<br>2.761<br>2.769 |
| $[Ca\{\mu^2\text{-}N(SiMe_3)_2\}\{N(C_6F_5)_2\}]_2$ (**5₂**)<br>Two distinct 3-coordinate Ca atoms | Ca1 | 2.4227<br>-<br>- | 2.477 |
| | Ca2 | 2.4560<br>-<br>- | 2.477 |
| $[\{BDI^{DiPP}\}CaN(C_6F_5)_2]_2$ (**7₂**)<br>Two identical 3-coordinate Ca atoms | Ca1 | 2.5325<br>2.5559<br>2.7120 | 2.581 [c]<br>2.584 [c]<br>2.612 [c] |
| $[Ca\{\mu\text{-}OB(CH(SiMe_3)_2)_2\}\{N(C_6F_5)_2\}]_2$ (**9₂**)<br>Two distinct 3-coordinate Ca atoms | Ca1 | 2.544<br>2.597 | 2.549<br>2.637 |
| | Ca2 | 2.498<br>2.553 | 2.551<br>2.583 |

[a] Measured interatomic distances to X = N, F or O atoms, given in Å; see Fig. 3, 4, 6 and 7 for detail.
[b] PBE0/Def2-TZVP-D3-optimised distances.
[c] Values calculated on the simplified **7'₂** model (see above).

Owing to the dominant electrostatic nature of the Ca···F–C interactions, the propensity for Ca to also trigger Ca···H–C non-ionic bonds raises the question of the nature of these interactions. Therefore, for the sake of comparison, the non-fluorinated equivalent of ***A***($CH_3F$), i.e. ***A***($CH_4$), was also investigated. Its optimised structure (Figure 9) exhibits a $\eta^3$-coordinated methane, with one shorter (2.621 Å) and two longer (2.817 Å) contacts. These values are commensurate with experimentally determined agostic Ca···H–C distances, e.g. 2.8933(6) Å in $[Ca\{N(SiMe_3)(mesityl).(thf)_2]$[34] and 2.7741(15) Å in $[Ca\{N(SiMe_3)(mesityl).tmeda]$.[34] The EDA data (Table 2) indicate substantially

weaker bonding in the ***A***($CH_4$) case (by more than 50%), but still with the same energy component order. Thus, the Ca···H–C interaction also has a major electrostatic and a weaker van der Waals character. Interestingly, the optimised structure of the ***A***($C_6H_6$) model (Figure 9) does not exhibit any Ca···H–C contact, but rather features a weakly $\eta^6$-coordinated benzene ligand (Ca–C = 3.054-3.165 Å). This indicates prevailing Ca···C(π) over Ca···H–C interactions, due to stronger covalent and van der Waals bonding (see Table 2). The interaction of calcium with a single unsaturated C=C bond is exemplified in the ***A***($C_2H_4$) model (Figure 9).The Ca–C distances (2.929 and 2.974 Å) are shorter than in ***A***($C_6H_6$). Its EDA values (Table 2) are very close to those of ***A***($CH_3F$), except for $E_{elstat}$ which indicates, as anticipated, weaker ionic bonding. Thus, amongst the various weak Ca···X (X = F, H, C(π)) interactions reported in the literature, our computations suggest that the Ca···F–C one appears to be the strongest, due to the high positive charge of $Ca^{2+}$ which in any case favours electrostatic interactions. This is in agreement with our earlier experimental findings, using structurally characterised alkyl-substituted complexes that display a range of Ca···F–C and Ca···C(π) interactions (as well as Ca···H–Si agostic contacts).[11a,11b,12e]

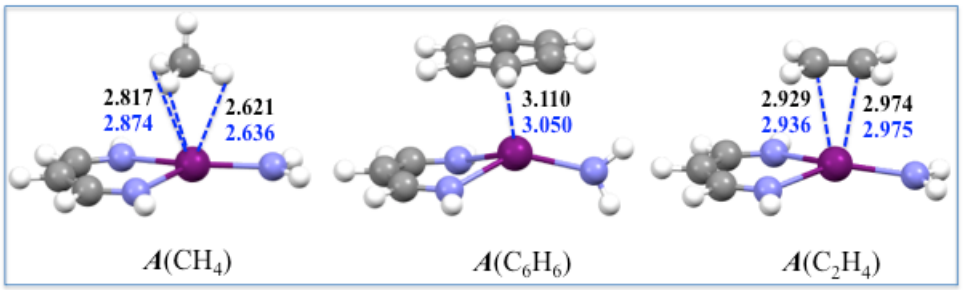


**Figure 9**. Optimised geometries of the ***A***($CH_4$), ***A***($C_6H_6$) and ***A***($C_2H_4$) models. Interatomic distances are given in Å; in black, with D3 corrections; in blue, without D3 corrections.

## Concluding remarks

Structural analysis of the several new [Ae]-$N(C_6F_5)_2$ complexes prepared herein for Ae = Ca and Ba demonstrate that Ae···F–C interactions are a convenient synthetic tool for the preparation of low coordinate complexes of the alkaline earths. The case of [{$BDI^{DiPP}$}$CaN(C_6F_5)_2]_2$ (**$7_2$**), where each $Ca^{2+}$ ion is formally three-coordinate, is particularly illustrative. Unlike the benchmark congener [{$BDI^{DiPP}$}$CaN(SiMe_3)_2$.(thf)], **$7_2$** does not contain coordinated thf; this would in most cases be beneficial for applications in catalysis. Besides, **$7_2$** is more readily accessed than the thf-free analogue, [{$BDI^{DiPP}$}$CaN(SiMe_3)_2$] (**3**), which has proved to be a most valuable synthetic precursor.[2j,6e,8] The molecular structures of the new complexes, with Ca–F interatomic distances around 2.50 Å or even shorter, indicate strong Ca···F–C intramolecular interactions, sufficiently so to allow the smooth formation of, for instance, compounds such as thf-free **$7_2$** and **$9_2$**. Complementary DOSY analysis

performed in benzene-$d_6$ at 25 °C (SI) suggests that *intermolecular* Ca···F–C interactions, and hence the dinuclear arrangement of these complexes, are retained in solution.

Although it is hence a useful synthetic tool in alkaline earth organometallic chemistry, the main drawback of the $N(C_6F_5)_2^-$ amide is its low basicity compared to that of more classical amides, e.g. $N(SiMe_3)_2^-$ or even $N(SiMe_2H)_2^-$. This limits the utilisation of [Ae]-$N(C_6F_5)_2$ complexes in molecular catalysis to the reactions where substrates are relatively acidic, e.g. phosphines in hydrophosphination, or where Brønsted acidity considerations are of little importance. This is illustrated for instance by the performances displayed by **$7_2$** in the hydroelementation catalysis. It proved inactive in the attempted intermolecular hydroamination of styrene with benzylamine, and in cyclohydroamination of 2,2-dimethylpent-4-en-1-amine, i.e. two reactions that [{BDI$^{DiPP}$}CaN(SiMe$_3$)$_2$.(thf)] catalyses very effectively.[2a,2d] On the other hand, **$7_2$** is an efficient precatalyst for the hydrophosphination of styrene with $HPPh_2$, affording near-quantitative formation of the *anti*-Markovnikov product of addition $PhCH_2CH_2PPh_2$ under experimental conditions (60 °C, 12 h, 10 mol-% precatalyst) that compare favourably with those required by the ubiquitous [{BDI$^{DiPP}$}CaN(SiMe$_3$)$_2$.(thf)] (75 °C, 20 h, 10 mol-% Ca).[35] On the whole, it can be concluded that although it is a convenient synthetic tool, $N(C_6F_5)_2^-$ is overall not ideally suited to Ae-mediated catalysis.

In view of these considerations, we have considered using the more basic $N(o\text{-}F\text{-}C_6H_4)_2^-$ as another stabilising, yet more reactive fluorinated arylamide. Preliminary results are encouraging. Following similar protocols to those implemented here, we have for instance been able to obtain [{BDI$^{DiPP}$}CaN(*o*-F-C$_6$H$_4$)$_2$.(thf)], a mononuclear complex that displays two strong intramolecular Ca···F–C contacts.[36] However, although we have spectroscopic evidence for its formation, we have not yet been able to crystallise the thf-free derivative [{BDI$^{DiPP}$}CaN(*o*-F-C$_6$H$_4$)$_2$]$_n$ that is required to carry out pertinent comparative catalytic studies. We have also been able to reproducibly isolate small crops of crystals of the tetranuclear $[Ca_4\{\mu^2\text{-}N(o\text{-}F\text{-}C_6H_4)_2\}_6\{N(SiMe_3)_2\}_2]$, a by-product in the reaction of $[Ca\{N(SiMe_3)_2\}_2]_3$ with $HN(o\text{-}F\text{-}C_6H_4)_2$. This unusual compound, certainly reminiscent of the trinuclear $[Ca\{N(SiMe_2H)_2\}_2]_3$,[10c] is also stabilised by very strong Ca···F–C interactions (SI), but the poor quality of the data and refinement preclude an informative discussion of metric parameters. The identity of the other compounds in this reaction have not yet been established, but optimisation of other reactions with $HN(o\text{-}F\text{-}C_6H_4)_2$ and related amines are still in progress in our laboratory and will be reported elsewhere.

DFT calculations have reproduced faithfully the molecular structures observed experimentally. A detailed bonding analysis of the Ca···F–C interactions indicate that its electrostatic component is largely predominant over of the covalent one, whereas dispersion forces are merely marginal. The $Ca^{2+}$ ion is not an efficient electro-acceptor centre and no significant F→Ca charge transfer occurs in the Ca···F–C interactions. On the other side, its highly charged nature confers it the ability of attracting substantial electronic density towards the interacting F atoms. Importantly, upon comparison of the relative strength of the three types of secondary interactions Ca···F(–C), Ca···H(–C) and Ca···C($\pi$) in model calcium

complexes, it emerges clearly that Ca···F–C is the strongest one; this is consistent with our experimental observations made in heteroleptic calcium fluoroaminoalkoxides.[11a,11b,12e] The combination of experimental and computational data presented here is an additional contribution to previous works that demonstrates the potential offered by non-covalent interactions in alkaline earth chemistry. We believe it is likely to open new opportunities to synthetic chemists with an imaginative mind, for instance to stabilise low-coordinated catalytic species.

## Supporting Information

Full experimental details; NMR spectra and crystallographic data for CCDC 1895996-1896001 and 1900852-1900853; details of DFT computations.

## Acknowledgements

H. R. is grateful to Erwann Le Coz for his assistance in the synthesis and crystallisation of complex **$6_2$.** The GENCI French national computer resource centre is acknowledged (grant A0050807367).

## Conflicts of interest

The authors declare no conflict of interest.

## Notes and references

[1] a) S. Harder, *Chem. Rev.* **2010**, *110*, 3852; b) M. R. Crimmin, M. S. Hill, *Top. Organomet. Chem.* **2013**, *45*, 191; c) M. S. Hill, D. J. Liptrot, C. Weetman, *Chem. Soc. Rev.* **2016**, *45*, 972; d) Y. Sarazin, J.-F. Carpentier, *Chem. Rec.* **2016**, *16*, 2482.

[2] See for instance: a) M. R. Crimmin, I. J. Casely, M. S. Hill, *J. Am. Chem. Soc.* **2005**, *127*, 2042; b) F. Buch, J. Brettar, S. Harder, *Angew. Chem. Int. Ed.* **2006**, *45*, 2741; c) J. Spielmann, F. Buch, S. Harder, *Angew. Chem. Int. Ed.* **2008**, *47*, 9434; d) A. G. M. Barrett, C. Brinkmann, M. R. Crimmin, M. S. Hill, P. Hunt, P. A. Procopiou, *J. Am. Chem. Soc.* **2009**, *131*, 12906; e) P. Jochmann, J. P. Davin, T. P. Spaniol, L. Maron, J. Okuda, *Angew. Chem. Int. Ed.* **2012**, *51*, 4452; f) B. Liu, T. Roisnel, J.-F. Carpentier, Y. Sarazin, *Angew. Chem. Int. Ed.* **2012**, *51*, 4943; g) M. D. Anker, M. Arrowsmith, P. Bellham, M. S. Hill, G. Kociok-Köhn, D. J. Liptrot, M. F. Mahon, C. Weetman, *Chem. Sci.* **2014**, *5*, 2826; h) C. Qi, V. Gandon, D. Lebœuf, *Angew. Chem. Int. Ed.* **2018**, *57*, 14245; i) H. Bauer, M. Alonso, C. Fischer, B. Rösch, H. Elsen, S. Harder, *Angew. Chem. Int. Ed.* **2018**, *57*, 15177; j) A. S. S. Wilson, C. Dinoi, M. S. Hill, M. F. Mahon, L. Maron, *Angew. Chem. Int. Ed.* **2018**, *57*, 15500.

[3] See for instance: a) J. Spielmann, G. Jansen, H. Bandmann, S. Harder, *Angew. Chem. Int. Ed.* **2008**, *47*, 6290; b) M. S. Hill, D. J. Liptrot, D. J. MacDougall, M. F. Mahon, T. P. Robinson, *Chem. Sci.*

**2013**, *4*, 4212; c) C. Bellini, J.-F. Carpentier, S. Tobisch, Y. Sarazin, *Angew. Chem. Int. Ed.* **2015**, *54*, 7679; d) E. Le Coz, V. Dorcet, T. Roisnel, S. Tobisch, J.-F. Carpentier, Y. Sarazin, *Angew. Chem. Int. Ed.* **2018**, *57*, 11747.

[4] a) S. Harder, F. Feil, K. Knoll, *Angew. Chem. Int. Ed.* **2001**, *40*, 4261; b) Y. Sarazin, B. Liu, T. Roisnel, L. Maron, J.-F. Carpentier, *J. Am. Chem. Soc.* **2011**, *133*, 9069; c) C. Bellini, C. Orione, J.-F. Carpentier, Y. Sarazin, *Angew. Chem. Int. Ed.* **2016**, *55*, 3744.

[5] See for instance: a) J. Spielmann, S. Harder, *J. Am. Chem. Soc.* **2009**, *131*, 5064; b) P. Jochmann, T. S. Dols, T. P. Spaniol, L. Perrin, L. Maron, J. Okuda, *Angew. Chem. Int. Ed.* **2010**, *49*, 7795; c) D. J. Liptrot, M. Arrowsmith, A. L. Colebatch, T. J. Hadlington, M. S. Hill, G. Kociok-Köhn, M. F. Mahon, *Angew. Chem. Int. Ed.* **2015**, *54*, 15280; d) V. Leich, T. P. Spaniol, L. Maron, J. Okuda, *Angew. Chem. Int. Ed.* **2016**, *55*, 4794; e) A. Causero, H. Elsen, J. Pahl, Sjoerd Harder, *Angew. Chem. Int. Ed.* **2017**, *56*, 6906; f) B. M. Wolf, C. Maichle-Mössmer, R. Anwander, *Angew. Chem. Int. Ed.* **2016**, *55*, 13893; g) M. D. Anker, C. E. Kefalidis, Y. Yang, J. Fang, M. S. Hill, M. F. Mahon, Laurent Maron, *J. Am. Chem. Soc.* **2017**, *139*, 10036; h) X. Shi, C. Hou, C. Zhou, Y. Song, J. Cheng, *Angew. Chem. Int. Ed*. **2017**, *56*, 16650; i) S. Brand, H. Elsen, J. Langer, W. A. Donaubauer, F. Hampel, S. Harder, *Angew. Chem. Int. Ed.* **2018**, *57*, 14169; j) B. M. Wolf, C. Stuhl, C. Maichle-Mössmer, R. Anwander, *J. Am. Chem. Soc.* **2018**, *140*, 2373; k) D. Mukherjee, T. Höllerhage, V. Leich, T. P. Spaniol, U. Englert, L. Maron, J. Okuda, *J. Am. Chem. Soc.* **2018**, *140*, 3403; l) H. Bauer, K. Thum, M. Alonso, C. Fischer, S. Harder, *Angew. Chem. Int. Ed.* **2019**, *58*, 4248; m) X. Shi, G. Qin, Y. Wang, L. Zhao, Z. Liu, J. Cheng, *Angew. Chem. Int. Ed.* **2019**, *58*, 4356.

[6] a) S. Harder, J. Brettar, *Angew. Chem. Int. Ed.* **2006**, *45*, 3474; b) C. Ruspic, S. Nembenna, A. Hofmeister, J. Magull, S. Harder, H. W. Roesky, *J. Am. Chem. Soc.* **2006**, *128*, 15000; c) S. Nembenna, H. W. Roesky, S. Nagendran, A. Hofmeister, J. Magull, P.-J. Wilbrandt, M. Hahn, *Angew. Chem. Int. Ed.* **2007**, *46*, 2512; d) M. P. Blake, N. Kaltsoyannis, P. Mountford, *J. Am. Chem. Soc.* **2011**, *133*, 15358; e) A. S. S. Wilson, M. S. Hill, M. F. Mahon, C. Dinoi, L. Maron, *Science* **2017**, *358*, 1168.

[7] B. Liu, T. Roisnel, J.-F. Carpentier, Y. Sarazin, *Chem. Eur. J.* **2013**, *19*, 13445.

[8] M. R. Crimmin, M. S. Hill, P. B. Hitchcock, M. F. Mahon, *New J. Chem.* **2010**, *34*, 1572.

[9] W. D. Buchanan, D. G. Allis, K. Ruhlandt-Senge, *Chem. Commun.* **2010**, *46*, 4449.

[10] a) K. Yan, B. M. Upton, A. Ellern, A. D. Sadow, *J. Am. Chem. Soc.* **2009**, *131*, 15110; b) Y. Sarazin, D. Roşca, V. Poirier, T. Roisnel, A. Silvestru, L. Maron, J.-F. Carpentier, *Organometallics* **2010**, *29*, 6569; c) N. Romero, S.-C. Roşca, Y. Sarazin, J.-F. Carpentier, L. Vendier, S. Mallet-Ladeira, C. Dinoi, M. Etienne, *Chem. Eur. J.* **2015**, *21*, 4115.

[11] a) S.-C. Roşca, C. Dinoi, E. Caytan, V. Dorcet, M. Etienne, J.-F. Carpentier, Y. Sarazin, *Chem. Eur. J.* **2016**, *22*, 6505; b) S.-C. Roşca, V. Dorcet, T. Roisnel, J.-F. Carpentier, Y. Sarazin, *Dalton*

*Trans.* **2017**, *46*, 14785; c) B. Freitag, J. Pahl, C. Färber, S. Harder, *Organometallics* **2018**, *37*, 469; d) L. Garcia, M. D. Anker, M. F. Mahon, L. Maron, M. S. Hill, *Dalton Trans.* **2018**, *47*, 12684.

[12] See references [4b], [10a], [11a], [11b] and: a) A. G. M. Barrett, M. R. Crimmin, M. S. Hill, P. B. Hitchcock, P. A. Procopiou, *Angew. Chem. Int. Ed.* **2007**, *46*, 6339; b) M. Gärtner, H. Görls, M. Westerhausen, *Dalton Trans.* **2008**, 1574; c) G. B. Deacon, P. C. Junk, R. P. Kelly, *Aust. J. Chem.* **2013**, *66*, 1288; d) S.-C. Roşca, T. Roisnel, V. Dorcet, J.-F. Carpentier, Y. Sarazin, *Organometallics* **2014**, *33*, 5630; e) S.-C. Roşca, E. Caytan, V. Dorcet, T. Roisnel, J.-F. Carpentier, Y. Sarazin, *Organometallics* **2017**, *36*, 1269.

[13] D. R. Click, B. L. Scott, J. G. Watkin, *Chem. Commun.* **1999**, 633.

[14] a) H. Yin, A. J. Lewis, U. J. Williams, P. J. Carroll, E. J. Schelter, *Chem. Sci.* **2013**, *4*, 798; b) H. Yin, A. J. Lewis, P. Carroll, E. J. Schelter, *Inorg. Chem.* **2013**, *52*, 8234; c) H. Yin, P. J. Carroll, E. J. Schelter, *Inorg. Chem.* **2016**, *55*, 5684; d) H. Yin, A. V. Zabula, E. J. Schelter, *Dalton Trans.* **2016**, *45*, 6313.

[15] J. F. Kögel, L. H. Finger, N. Frank, J. Sundermeyer, *Inorg. Chem.* **2014**, *53*, 3839.

[16] J. F. Kögel, D. A. Sorokin, A. Khvorost, M. Scott, K. Harms, D. Himmel, I. Krossing, J. Sundermeyer, *Chem. Sci.* **2018**, *9*, 245.

[17] a) I. D. Brown, D. Altermatt, *Acta Crystallogr. Sect. B* **1985**, *B41*, 244; b) N. E. Brese, M. O'Keefe, *Acta Crystallogr., Sect. B* **1991**, *B47*, 192; c) I. D. Brown, *Chem. Rev.* **2009**, *109*, 6858.

[18] R. Koppang, *Acta chem. Scand.* **1971**, *25*, 3067.

[19] J. Eppinger, E. Herdtweck, R. Anwander, *Polyhedron* **1998**, *17*, 1201.

[20] M. P. Coles, *Coord. Chem. Rev.* **2016**, *323*, 52.

[21] M. Westerhausen, M. Hartmann, N. Makropoulos, B. Wieneke, M. Wieneke, W. Schwarz, D. Stalke, *Z. Naturforsch., B: Chem. Sci.* **1998**, *53*, 117.

[22] H. Plenio, *Chem. Rev.* **1997**, *97*, 3363.

[23] M. Westerhausen, W. Schwarz, *Z. Anorg. Allg. Chem.* **1991**, *604*, 127.

[24] T. J. Boyle, B. A. Hernandez-Sanchez, C. M. Baros, L. N. Brewer, M. A. Rodriguez, *Chem. Mater.* **2007**, *19*, 2016.

[25] A. G. M. Barrett, M. R. Crimmin, M. S. Hill, G. Kociok-Köhn, D. J. MacDougall, M. F. Mahon, P. A. Procopiou, *Organometallics* **2008**, *27*, 3939.

[26] H. Bauer, M. Alonso, C. Färber, H. Elsen, J. Pahl, A. Causero, G. Ballmann, F. De Proft, S. Harder, *Nat. Catal.* **2018**, *1*, 40.

[27] A search on the CSD database (version 5.40) for 3-coordinate charge neutral calcium compounds returned 14 hits: CSD entries ABAGOA, CUDZUX, CULMAX, EPENIY, FISWEK, JOFPID, LIDFAF, LOSPOY, PUVGAP, TERGIH, VEMNAF, YOGYAV, YOGYEZ and YUMBAT.

[28] B. A. Vaartstra, J. C. Huffman, W. E. Streib, K. G. Caulton, *Inorg. Chem.* **1991**, *30*, 121.

[29] a) S.-O. Hauber, F. Lissner, G. B. Deacon, M. Niemeyer, *Angew. Chem. Int. Ed.* **2005**, *44*, 587; b) O. Michel, S. König, K. W. Törnroos, C. Maichle-Mössmer, R. Anwander, *Chem. Eur. J.* **2011**, *17*, 11857.

[30] B. Liu, T. Roisnel, Y. Sarazin, *Inorg. Chim. Acta* **2012**, *380*, 2.

[31] a) W. D. Buchanan, E. D. Nagle, K. Ruhlandt-Senge, *Main Group Chem.* **2009**, *8*, 263; b) J. S. Sum, L. Tahsini, J. A. Golen, C. Moore, A. L. Rheingold, L. H. Doerrer, *Chem. Eur. J.* **2013**, *19*, 6374; c) W. D. Buchanan, K. Ruhlandt-Senge, *Chem. Eur. J.* **2013**, *19*, 10708.

[32] S. Grimme, S. Ehrlich, L. Goerigk, *J. Comp. Chem.* **2011**, *32*, 1456.

[33] a) K. Morokuma, *J. Chem. Phys.* **1971**, *55*, 1236; b) T. Ziegler, A. Rauk, *Inorg. Chem.* **1979**, *18*, 1558; c) F. M. Bickelhaupt, E. J. Baerends, *Rev. Comput. Chem*.; K.B. Lipkowitz and D.B. Boyd, Eds.; Wiley, New York **2000**, *15*, 1.

[34] M. Gillett-Kunnath, W. Teng, W. Vargas, K. Ruhlandt-Senge, *Inorg. Chem.* **2005**, *44*, 4862.

[35] M. R. Crimmin, A. G. M. Barrett, M. S. Hill, P. B. Hitchcock, P. A. Procopiou, *Organometallics* **2007**, *26*, 2953.

[36] The molecular structure of [{BDI$^{DiPP}$}CaN(*o*-F-$C_6H_4$)$_2$.(thf)] is given in the Supporting Information. The data set and final refinement we have so far been able to achieve are of insufficient quality to discuss the details of interatomic distances and angles ($R_{int}$ = 0.1638, $R_1$ = 0.0978), but the connectivity was established without ambiguity.

10.1002/chem.201901262

**Graphical Abstract**

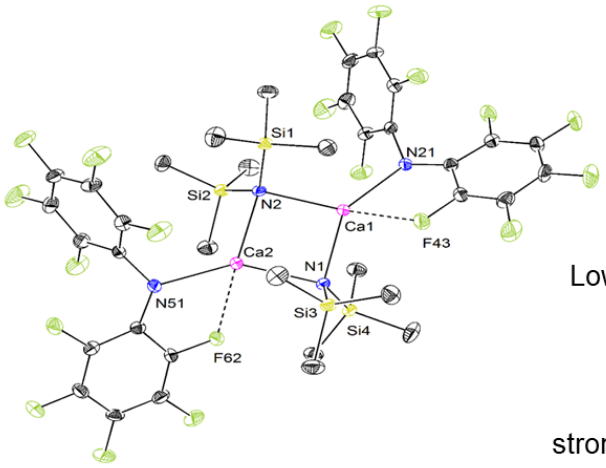


Low coordinate calcium and barium complexes
+
fluoroarylamides
=
strong metal···F-C interactions